Model validation and dynamic simulation of post-combustion carbon dioxide separation with membranes

Antonio Tripodi, Renato La Pietra, Matteo Tommasi, Ilenia Rossetti*

Chemical Plants and Industrial Chemistry Group, Dip. Chimica, Università degli Studi di Milano, CNR-SCITEC and INSTM Unit Milano-Università, via C. Golgi 19, 20133 Milano, Italy

Abstract

This work presents a finite-element numerical model for N_2-O_2-CO_2 separation by hollow fiber membranes, scaled-up to treat the combustion gases coming for a medium-size coal-based power unit. The equation set has been expanded to include, beyond the membranes, also compressors and condensers. Two process layouts have been evaluated: one open loop allowing for high purification level, and a recirculating scheme yielding superior enrichments. The resulting simulation, valid from pilot to full-plant scale, takes then into account the interplay of both active and passive process units besides the active membranes, and is fully dynamic in definition and scope.

The results show that the degree of purification is mainly affected by the enrichment-side pressure, while the CO_2 concentration depends largely on the CO_2:N_2 selectivity. Even when this latter value is relatively low, a proper scale-up of series/parallel modules can overcome the limitation without exceeding 7 – 8 bar pressurisation. Simulating the impact of pressure and flow transients on the plant outflows, the recovery procedure and timescales are identified.

Keywords: Carbon Capture; CO_2 sequestration; CO_2 separation; Membrane separation; Dynamic simulation.

* Corresponding author: fax +39-02-50314300, email ilenia.rossetti@unimi.it

1 - Introduction

As carbon capture has gained importance, both within an environmental impact and atom-economy perspectives, waste-gases produced by power plants can be treated by pre-combustion, oxy-combustion, or post-combustion strategies [1]. Oxy-combustion is limited by the need of pure oxygen, which in turn can be energy-demanding (if obtained by distillation) or requires additional separation plants; the second issue belongs also to the pre-combustion approach. Post-combustion approach, on the other hand, foresees simpler plant layouts, but on the other hand yields lower concentrations of CO_2 in the effluents. It is nonetheless considered a very promising technology because it can be easily retrofitted to existing power plants [1–3].

The separation of carbon dioxide via membranes is very attractive as it needs virtually no thermal inputs. It is preferentially applied to gases with a CO_2 content of 10 – 20% vol [4], because very diluted mixtures would require a high specific compression power [5], while for already pre-concentrated streams cryogenic processes become viable [6]. A first section usually purifies the plant effluents, while a second one enriches the carbon dioxide stream [7]. This technology does not require other chemicals (amines, salts, physical solvents) to be purchased and stored. Membranes packages can also be easily adapted to a wide range of process scales [8], and do not need the regeneration cycles typical of solid adsorbents (which imply larger capital expenses and the extra equipment needed by coupling batch with continuous processes). The main disadvantages of the membrane-based capture are the relatively low purity of the captured CO_2, and the need to remove water [9] and other species potentially non-compatible with the membranes material [10,11].

Ongoing research has made available a variety of materials and shapes with ever increasing selectivity and packing efficiency [12]. Fiber membranes folded in hollow cylinders, in turn arranged into modules composed of $10^3 – 10^5$ stems, feature a very high active surface per element, 10 to 100 times larger than other membranes types [13,14] and can be well represented by mono-dimensional models using the cylinder axis as the only spatial coordinate, thanks to their small radius. The very high

thickness-to-radius ratio, on the other hand, decreases their permeability and makes them sensitive to water condensation (unless they are used as contactors to enhance the transport coefficient of gas-liquid applications [13,15,16]), so a reliable simulation for the gas-gas technology must consider separating devices.

Simulation works related to the whole separation process usually account for plants steady states [17,18], while more accurate dynamic calculations are often employed to treat a membrane's inner behavior [19] or pilot-scale single elements [20].

To fill this gap, in this work, a fully dynamic simulation is extended to a whole separation plant, except for the CO_2 enrichment part, after validating and scaling-up a model built to represent a single bench-scale module. This allows to foresee the off-design plant conditions that are the outcomes of transient behaviors. The strategy is the adoption, as basic process units, of membrane stacks made of parallel modules. The conservative permeance values (under 100 GPU for CO_2, in the low-performance range of the materials reviewed in [5,21,22]) of a polymeric hollow fiber have been selected, nonetheless coupled to very large available surfaces and an average CO_2:N_2 selectivity of 30 [21,23].

The treated gas is a stream coming from the combustion of coal. A power plant of 607 MW_{el} (Neurath Unit 4 [24]) is taken as reference and the gas flow and composition have been estimated by the plant fuel consumption and lignite composition analysis [10].

2 – Methods

The simulation of the membrane adsorption has been carried out with an equation-oriented approach, using Aspen Custom Modeler v8 by Aspen Tech [25]. This software allows defining and solving a linear system of first-order (with respect to time) differential equations, plus algebraic equations and boundary conditions. Moreover, the steady state solutions (equivalent to the convergence points of a steady-state process simulation) can be sought independently by setting to zero all the time

derivatives, without waiting for the variables to complete their dynamic from a non-stable initial point. The algebraic and differential equations are solved by separate sub-calculators.

In the model developed for this work, a finite-element approach has been used to represent the membrane modules, rather than resorting to partial differential equations. The integration method selected – already provided by the software – is the one by Gear [26], preferred to the default choice (implicit-Euler).

The process simulation has been carried out through the following steps:

a. choice of a dynamic model for the membranes and its translation into the Aspen Custom Modeler proprietary programming language, defining an independent "membrane module" subsystem;
b. validation of the model translation, checking the results when using the same process conditions defined by the original models;
c. choice of a model for the flue gas compressor and reimplementation of the equations;
d. steady-state solution of the compressor model for a reference performance curve (see "scale-up" paragraph) and comparison of the gas flow with the rated hydraulic conditions of a membrane;
e. scale-up of the membrane model active surface by two orders of magnitude, to align it with the gas flow calculated by the compressor model;
f. further modelling of mixers, splitter (they distribute the gas between two-three parallel membrane trains), and water condenser;
g. process design by connection of the appropriate number of blocks, modifying at need the compressors curves and the condenser geometries and duties.

The compressor is modeled after the work of Venturini [27], that uses two polynomial interpolation of the characteristic and efficiency curves and deals with mass accumulation and shock-waves across the unit. The condenser model accounts for three phenomena: 1) liquid and vapor separation according to the thermodynamic equilibrium (at fixed volume and mixture composition), 2) heat

exchange via an overall heat transfer coefficient (at fixed imposed outer temperature) and 3) influence of the vessel geometry on the vapor velocity (which has to be low enough to minimize the liquid entrainment). The only simplifying assumption is that the transport at the vapor-liquid interface is instantaneous.

The mixer and splitter models are meant to be used always together, to represent a fluid header with multiples inlet/outlets, so only the mixing part is assigned a non-zero volume with ensuing dynamic behavior, while the mixing part acts just as a routing for the outlets. Other details are in Table *2*.

3 - Membrane model validation

The developed model is based on the approach by Coker [23], that adopts the following further assumptions:

- the membranes are treated with mean transport coefficients depending only on the chemical species, hiding the detailed dependences on thickness, pore sizes and diffusion coefficients;
- the process is isothermal;
- the transport driving force depends on the partial pressures, that are in turn calculated by the perfect gas law without non-ideality effects;
- a membrane module is represented by ten sub-modules placed in series (and connected with retentate and permeate either in counter-current or co-current arrangements): each sub-module is considered in mixed-flow conditions; in this way the spatial domain is discretized, and not considered as a variable in the differential equations solution.

According to the above-mentioned reference work, the model has been set-up and validated for a case of air purification, nevertheless the cited authors give a set of transport coefficients valid also for the other chemical species involved in flue gas purification (see Table *1*). We tested the model with an air-separation case, not with CO_2 separation case of study, because the original finite-element formulas were not fully disclosed in the cited reference and were solved with a different software and a different mathematical technique. Through this preliminary

validation we ensured that the same finite-element approach and the same permeability values yielded the same results, ruling out pure mathematical differences.

The same mathematical model has been used also by other authors [28], who reported also comparable ranges for gases permeability and selectivity. An implementation with the Aspen Custom Modeler software has also been carried out by Scholz et al. [29] for a CO_2-CH_4 case study. The geometrical details regarding a membrane module can be found in the referenced paper, while the comparison of the original model (lines) and the test calculation of the present work (points) are found in Figure 1.

Main membrane parameters [23]	
Pressure	0 – 10 bar
Membrane type	Hollow fiber
CO_2 Permeability	10 – 100 GPU
CO_2:N_2 selectivity	30 GPU/GPU
O_2:N_2 selectivity	5.6 GPU/GPU
Specific surface	1500 m^2/m^3

Table 1: Main membrane parameters from the reference work [23]. 1 GPU = 10^{-6} std-cm^3 cm^{-2} s^{-1} cm_{Hg}^{-1} = 7.501×10^{-12} std-m^3 m^{-2} s^{-1} Pa^{-1} = 3.346×10^{-13} kmol m^{-2} s^{-1} Pa^{-1}.

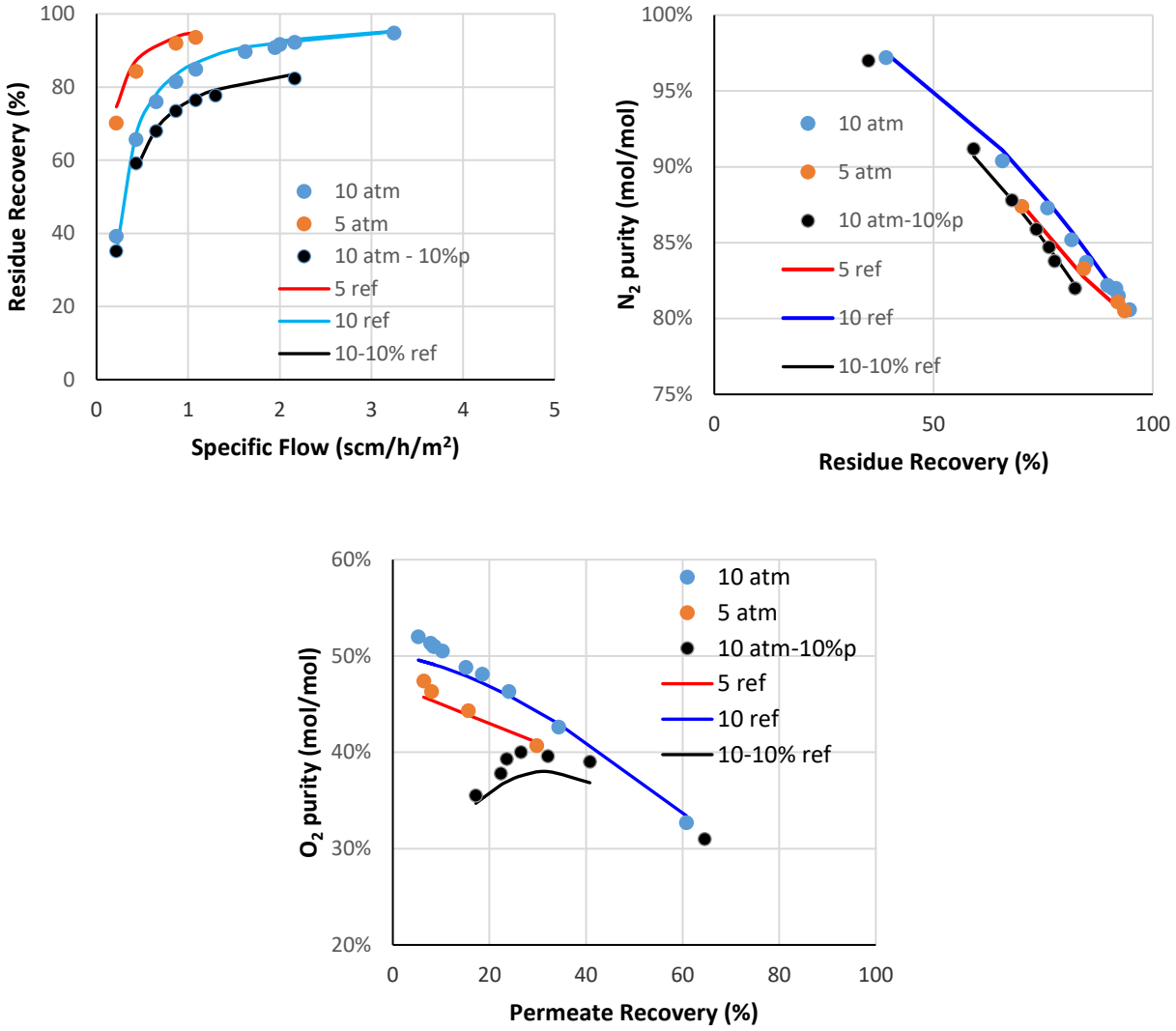

Figure 1: Evaluation of the model re-implementation behavior with respect to the original formulas for the case of air separation: the lines represent the results of Coker et al. [23], the circles are from this work calculations.

The variation of membranes permeability and selectivity according to temperature [30,31] will be considered in further works. The differential and algebraic equations used to set-up this simulation are listed in Table 2.

n	block	equation
1		$\frac{dn_{i,Ret}}{dt} = RET_{IN} z_{i,Ret_{IN}} - RET_{OUT} z_{i,Ret} - J_i$
2	membrane	$\frac{dn_{i,Per}}{dt} = PER_{IN} z_{i,Per_{IN}} - PER_{OUT} z_{i,Per} + J_i$
3		$J_i = S \; v_{Ret} G_i \left(p_R z_{i,Ret} - p_P z_{i,Per} \right)$

4		$\frac{1}{f} = 4\log_{10}\left(\frac{\varepsilon}{3.7D_{Ret}} + \frac{2.51}{Re_{Ret}f^{1/2}}\right)$
5		$\left(p_{Ret,IN} - p_{Ret}\right) = 0.433\, f \frac{v_{Ret}}{A_{Ret}^{3/2}} \rho_{Ret} u_{Ret}^2$
6	Water separator	$\frac{dn_i}{dt} = Fz_i - Lx_i - Vy_i$
7		$\frac{dH}{dt} = Fh - Lh_L - Vh_V + Q$
8		$Q = -UA(T - T_{amb})$
9		$F = CV_{IN}(P_{IN} - P)$
10		$V = CV_V(P - P_{amb})$
11		$L = CV_L(P - P_{amb})$
12		$\varphi = \frac{L \times PM_L}{V \times PM_V}\left(\frac{\rho_V \times PM_V}{\rho_L \times PM_L}\right)^2$
13		$k = 0.01 + \frac{0.3\varphi^{0.7}}{0.03+\varphi} e^{-0.6\varphi}$
14		$u_{max} = k\sqrt{\frac{\rho_L \times PM_L}{\rho_V \times PM_V}}$
15	compressor	$W = \frac{F_{out}}{3600}\frac{\gamma}{\gamma - 1} RT_{in}\left[\left(\frac{P_{out}}{P_{in}}\right)^{\frac{\gamma-1}{\eta\gamma}} - 1\right]$
16		$\eta = \eta_1 + \frac{\eta_3}{\left[\frac{F_{out}}{PM} \times \frac{RT_{in}}{P_{in}} - \eta_2\right]^{\eta_4}}$
17		$T_{out} = T_{in}\left(\frac{P_{out}}{P_{in}}\right)^{\frac{\gamma-1}{\eta\gamma}}$
18		$\frac{P_{out}}{P_{in}} = p_1 + \frac{p_3}{\left[\frac{F_{out}}{PM} \times \frac{RT_{in}}{P_{in}} - p_2\right]^{p_4}}$
19		$\frac{dF_{in}}{dt} = \frac{A_{suc}}{L_{suc}}(P_{suc} - P_{in})$
20		$\frac{dP_{in}}{dt} = \gamma RT_{in}\frac{F_{in} - F_{out}}{PM \times v_{cmpr}}$

Table 2: List of the equations used in the model. See the list of symbols. The membrane friction factor is calculated with the Coolebrok formula. The compressor efficiency and pressure ratio are fitted with rational functions, while its momentum balance is calculated after [27]. The vapor velocity correction factor is interpolated after [32].

4 - Process layout and scale-up

Due to the fact that the compressor model is rigorous, its reliability depends on the use of actual performance curves, so its size has to be chosen as the maximum one for which such details are available in the open literature or undisclosed industry reports. A further constrain is the choice of data for the simulated range of pressures only. This has brought to model a unit [33] that can treat roughly one tenth of the above mentioned gas flow, implying that the cost of the simulated process should be rescaled. Though larger machines are available on the market, we could not obtain detailed performance curves.

The membrane model is scaled-up placing only ten sub-modules in series, but supposing to handle larger stacks of 100 modules in parallel, with the retentate (and permeate) side in perfect radial mixing conditions: this means that, for the same sub-module length, the active surface, the sides hydraulic sections and volumes are multiplied by 100. This size has been chosen judging that the resulting scale-up of the shells-side (retentate) hydraulic radius would be not so important as to impose to reconsider the model. Then other stacks are placed in series to achieve the desired separation level.

As a result, the gas flow handled by a scaled-up stack accounts for about a half of the selected operating point in the used performance curve (Figure 4) for a high pressure level of 6 – 7 bar, which in turn is well within the membrane model validation range. The details are found in Table *4* for the nominal working point.

The separation layout follows two designs: a simple once-through scheme (Figure 2) and one where the combustion gases are re-diluted with recirculating air (resembling the schemes where the combustion chamber is fed with air from the membranes [34,35], or the ones where undiluted permeate is recycled [36]; see also Figure 3): this latter configuration requires additional membrane surface to accommodate the larger flow ensuing. The direct sweep gas (almost all nitrogen) mixing

to the flues allows to simulate the furnace feeding by air used for CO_2 purification, but without modeling also the combustion section and also varying the gas flows without the need to respect the N_2:O_2:C proportion imposed by the stoichiometry.

Since this work is focused on the model development and dynamic behavior, other possible configurations will be considered in further works. Alternative possible designs are exemplified in references [31–33,35].

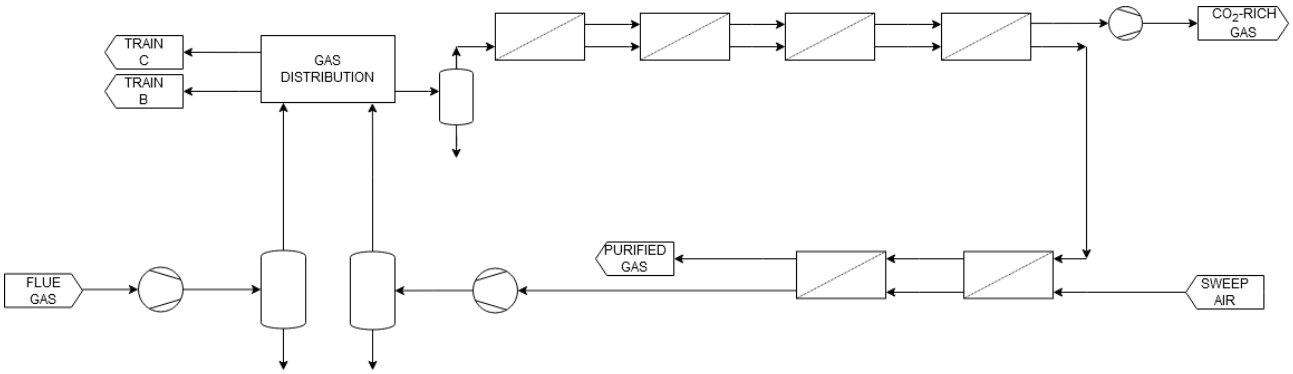

Figure 2: Layout with recycle.

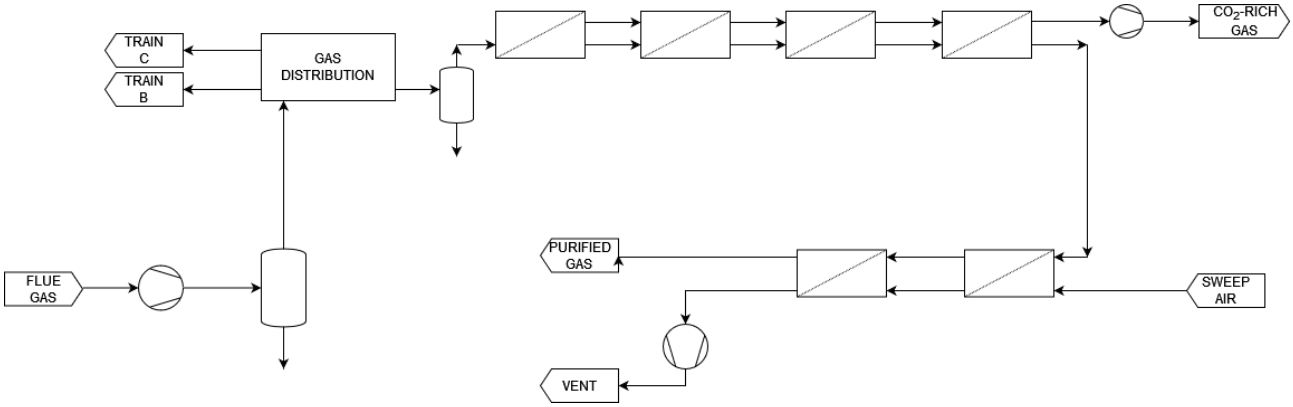

Figure 3: Layout without recycle.

The sweep air compressor is modeled in the same way as the flue unit, and in this case the performance curve used has been taken from the literature [37], the needed pressure level is reached in two stages.

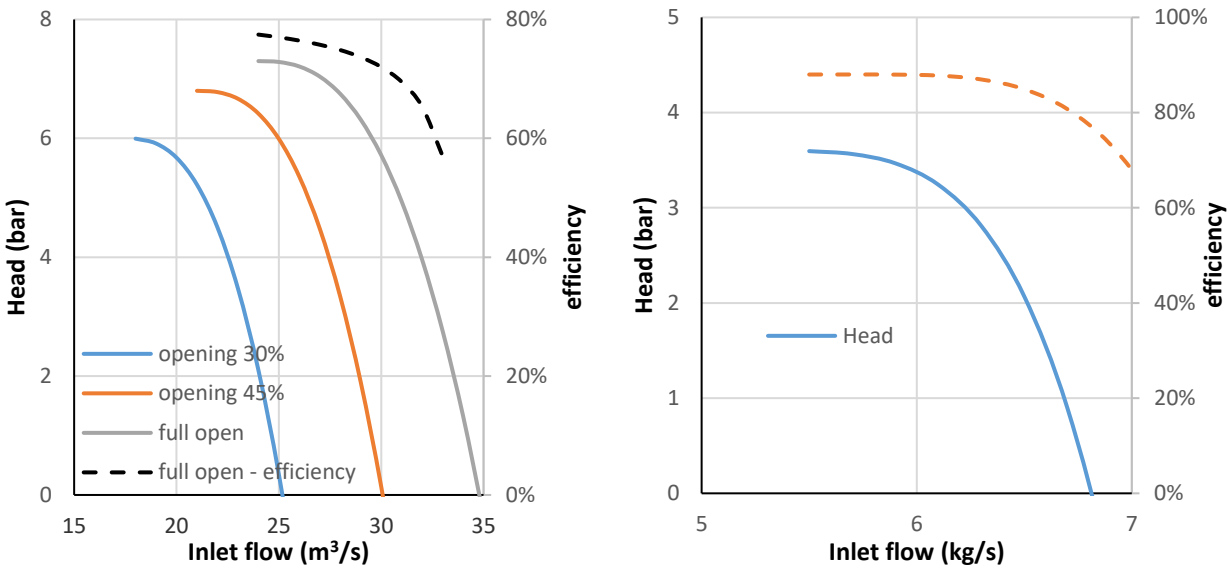

Figure 4: (left) large and (right) small compressors curves.

The scale-up of the process has brought to define the input data and main parameters values reported in

Table 3

Table *3* and

Table *4*. With the permeate side kept at sub-atmospheric pressure, the waste gas can be compressed to mild levels (below 10 bar) to ensure a good operation [31]. A very interesting comparison about process layouts and mixtures compositions has also been done by Merkel et al. [38].

	Flues	**Sweep gas**
CO_2	0.201	0.01
N_2	0.741	0.98
H_2O	0.058	0.01

Table 3: Simulation input streams composition (mass fractions).

		Membrane module	Module stack	Flue compressor	Air compressor	Plant Unit	Compressor per unit	Stacks per compressor
				Configuration with recycle (Figure 2)				
Flue gas	**scm/s**	0.0784	7.84	28.5	0.00	418	15	4
Sweep gas	**kg/h**	200	20000	0.00	20000	300000	15	2
Recycle	**scm/s**	0.0556	5.55	0.00	0.00	296		
Total flow	**scm/s**	0.134	13.4	28.5	20000	714	30	6
Reference flow	**scm/s**	0.140	14.0	24.0 – 34.0	-	746	-	-
				Configuration without recycle (Figure 3)				
Flue gas	**scm/s**	0.0784	7.84	28.5	0.00	418	15	4
Sweep gas	**kg/h**	200	20000	0.00	20000	300000	15	2
Total flow	**scm/s**	0.0784	7.84	28.5	20000	418	30	6
Reference flow	**scm/s**	0.140	14.0	24.0 – 34.0	-	418		

Table 4: Reference design points for the configurations of Figure 2 and Figure 3. scm = m^3 measured in standard conditions (i.e. 298 K, 1 atm).

5 - Simulation results

The results presented are relative to six different dynamic scenarios, all starting and ending with a steady state. The variations of the tested process variables are listed in Table 5, while several rated plant working points belonging to each run are listed in Table 6.

Dynamic 1				**Dynamic 2**			
Hours	Variable	Action	Final state	Hours	Variable	Action	Final state
0-2	-	wait	1	0-2	-	wait	1
2-3	flow	Ramp to 110%	-	2-3	flow	Ramp to 110%	-

3-10	-	wait	2	2.5-3.5	Sweep air	Ramp to 90%	-
10-11	Sweep air	Ramp to 105%	-	3-3.5	Vacuum	Ramp to 90%	-
11-21	-	Wait	3	3.5-24	-	Wait	11
21-22	Sweep air	Ramp to 95%	-				
22-40	-	Wait	4				
40-41	Vacuum	Ramp to 90%	-				
41-60	-	Wait	5				
Dynamic 3				**Dynamic 4**			
Hours	Variable	Action	Final state	Hours	Variable	Action	Final state
0	-	-	11	0-1	-	Wait	1
0-2	Compression	Ramp to 107%	-	1-5	Condenser outlet Cv	Ramp to 33%	20
2-12	-	wait	12	5-6	Vacuum	Ramp to 90%	-
12-12.5	Vacuum	Ramp to 75%	-	6-11	-	Wait	21
12.5-24	-	Wait	13				
Dynamic 5				**Dynamic 6**			
Hours	Variable	Action	Final state	Hours	Variable	Action	Final state
0-2	-	Wait	50	0-2	-	Wait	50
2-3	flow	Ramp to 120%	51	2-3	Vacuum	Ramp to 350%	-

3-3.5	Vacuum	Ramp to 75%	-	3-4	-	Wait	61
3.5-6	-	WAIT	52	4-6	flow	Ramp to 75%	62
6-8	Condenser inlet Cv	Ramp to 5000	-	6-12	-	wait	63
8-24	-	Wait	53				

215 Table 5: Dynamic simulation schedules.

216

Case	**Scheme**	**sequence**	**Purified flow**	**CO_2**		**Pressure**		**Compr Duty**
				Purity	recovery	Retentate	Permeate	
			kmol/h	Mol/mol	(%)	bar		kWe
1	recycle	1	1395.5	0.009270	94.087	6.5957	0.25	14253
2	recycle	1	1475.8	0.01040	90.757	6.5763	0.25	14255
3	recycle	1	1512.2	0.01083	92.531	6.569	0.25	14335
4	recycle	1	1439.6	0.01017	93.009	6.5836	0.25	14176
5	recycle	1	1437.8	0.009530	93.972	6.584	0.22	14172
11	recycle	2-3	1400.5	0.008768	96.33	6.5916	0.2	14086
12	recycle	3	1378.7	0.007224	93.98	7.0901	0.2	14315
13	recycle	3	1381.2	0.008123	96.33	7.0894	0.25	14322
20	recycle	4	1685.6	0.01615	93.39	5.6487	0.25	14747
21	recycle	4	1429.1	0.01143	84.438	5.7873	0.2	14216
50	open	5	561.9	0.002883	93.852	6.7713	0.25	14240
51	open	5	745.42	0.003691	93.101	6.7275	0.25	14306
52	open	5	742.54	0.003593	84.928	6.7275	0.2	14239
53	open	5	757.68	0.004197	91.256	6.4787	0.2	14230
61	open	6	567.83	0.006415	81.952	6.7771	0.95	14293
62	open	6	394.81	0.006513	72.625	6.8184	0.95	14243
63	open	6	395.54	0.005818	94.039	6.8183	0.95	14271

217 Table 6: Simulation results for rated working points

As expected, the open-cycle cases grant CO_2 fractions always below 1%, but with poorer recoveries. The compressor duties are instead similar because the layout difference impacts only on the enriched gas compressor. In general, closed configurations (with recycle) might be preferred because the carbon content of the flues is still small and higher recoveries make a better option for possible downstream CO_2 reuse.

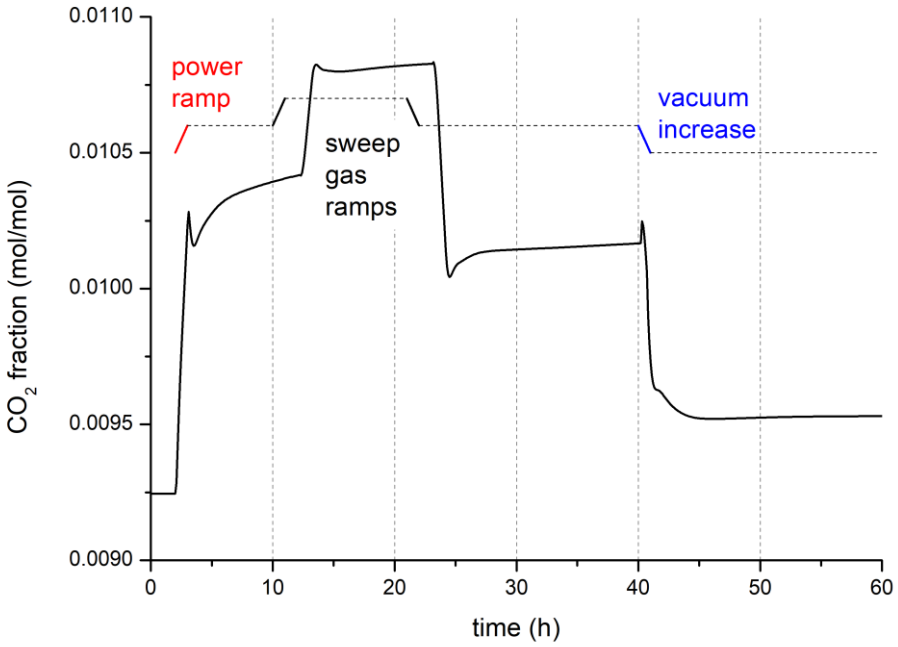

224

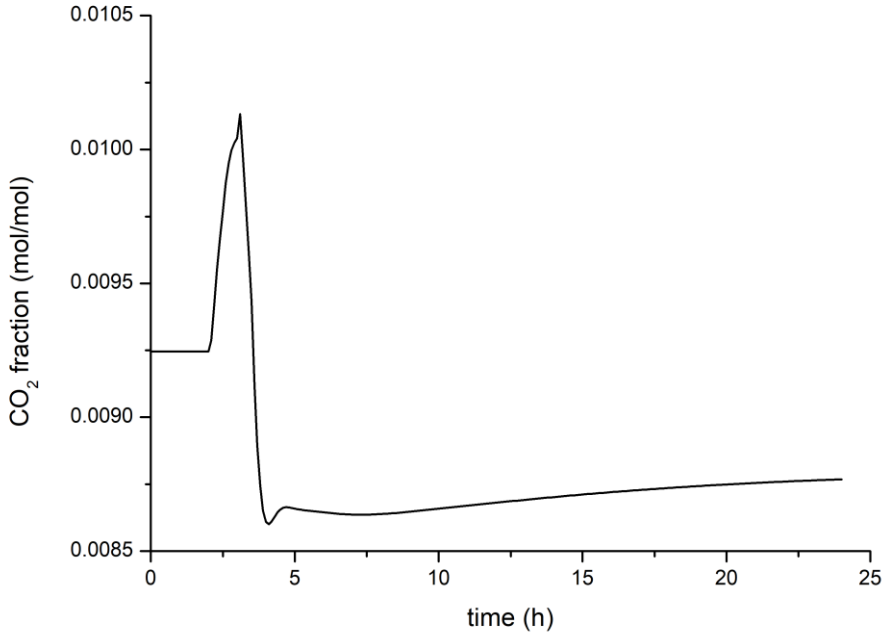

225

226 Figure 5: CO_2 fractions in the purified flues for the simulation schedules 1-2. The top graph shows also the occurrence

227 of the process parameters variations along the timeline.

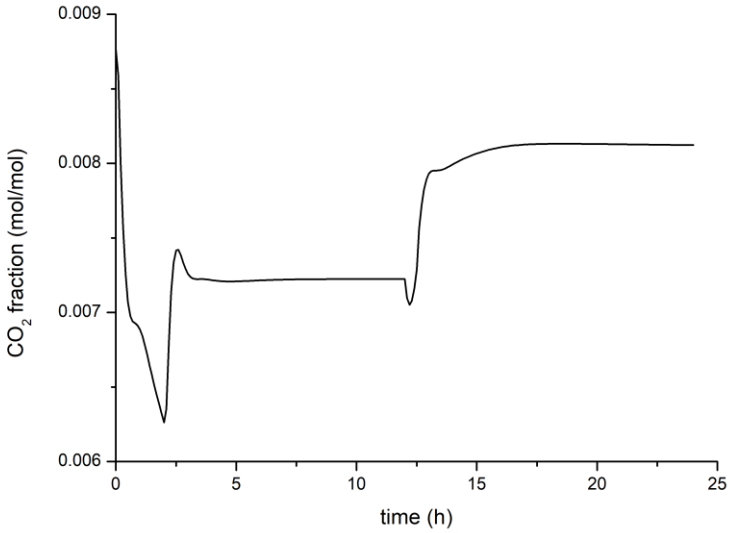

228

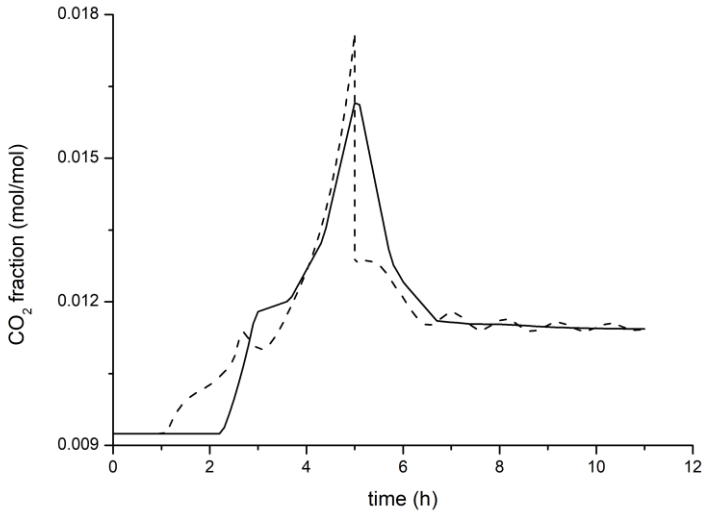

229

230 Figure 6: CO_2 fractions in the purified flues for the simulation schedules 3-4. For the fourth run, the dotted line
231 represents the numerical solution with the default integration options, that had to be obtained breaking the time-flow
232 and accumulating a series of steady-state solutions in several critical passages; the continuous line represents a smooth-
233 running solutions obtained introducing a lowpass numerical filter in the form of fixed expanded integration steps.

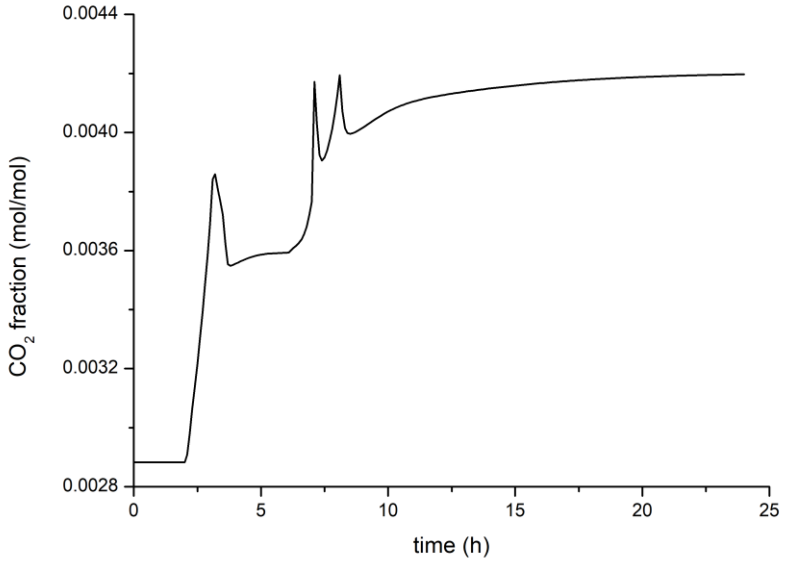

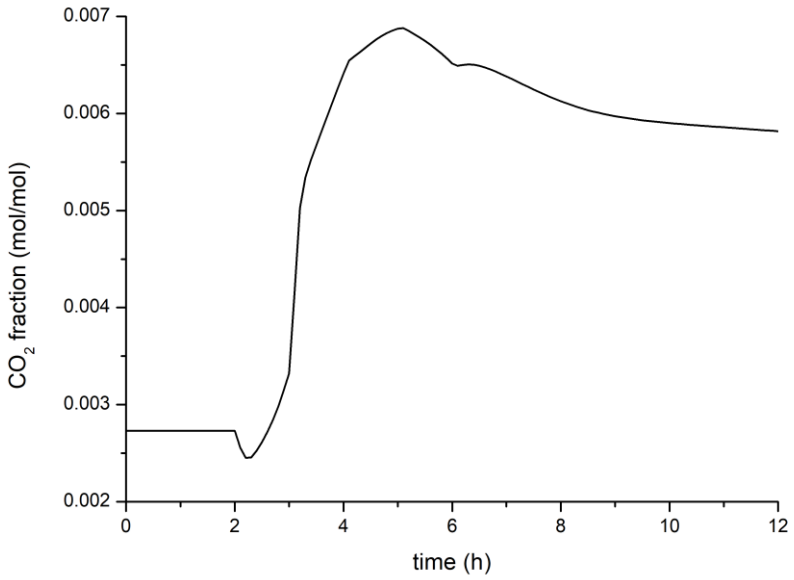

Figure 7: CO_2 fractions in the purified flues for the simulation schedules 5-6. The sixth run was run with the same noise-damping strategies adopted for the fourth.

The trend obtained for the dynamic 1 simulation (Fig. 5) shows that an increase in plant power (e.g. in flues emission), can be compensated by a reduced recycle flow, and not an increase, because we consider the purge gas as containing a fraction of CO_2. Variations of a 10% in the permeate vacuum level (last part of dynamic 1 and dynamic 2) have, instead, a minor effect.

The third schedule shows the effect of an increase in the membrane operating pressure: the interesting feature is the relatively high difference in the transient and steady state purification levels achieved, 0.66% and 0.73% vol. respectively (with respect to the rated 0.88%), which can be appreciated only having set up a full dynamic calculation for compressors and separators beside membranes. In this case, the relative effect of a moderate vacuum loss is appreciable.

On the other hand (dynamic 4) a reduced working pressure can even double the nominal CO_2 content: this dynamic run has highlighted several model criticalities that depends strictly on the mathematical problem, and can remain hidden according to the boundary conditions and variations tested. In this case, the step-change imposed to the system pressure first derivative (at the end of the ramp), results in a too big numerical oscillation for the flow in the sweep-air compression modules. This problem is numerical, because steady solutions are always promptly calculated (as any tested pressure value still belongs to the compressor operating range). The approach used by the default integration package is to reduce dynamically the integration step size when discontinuities are encountered, in order to proceed gradually from one state to the other, but in this case the enhanced resolution in the time domain results in further numerical oscillations. The issue has been solved in two ways: a) stop the pressure ramp just before the step-change of the pressure derivative, then solve the steady state and resume the dynamic; b) impose a fixed integration time large enough to damp the numerical oscillation.

Dynamic 5 highlights again the differences between transient and stabilized value following power surges and vacuum losses (but without recycles), and dynamic 6 simulates a total vacuum loss, which can be taken as a design accident (stemming from a power loss or line big leak) for the permeate side of the separation plant.

The process layout with recycled air yields systematically higher CO_2 fractions in the treated gas, because the membranes have to treat a larger quantity of N_2, on the other hand this value is less sensitive (on relative terms) to variations in the process parameters. Both the co-current and counter-current membrane arrangements separate the larger part of the CO_2 flow in their inlet zone.

Also the sixth dynamic run presented numerical problems similar to those of the fourth schedule, and has been run at fixed integration steps. These limitations could come from the fact that the adopted models mix a "flow driven" approach (the membranes, that inherit a fixed flow and yield the resulting pressure) with a "pressure driven" one (the compressors and the condensers, that require fixed outlet pressures). Moreover, there is not a unique combination of boundary conditions (fixed pressure and flows) yielding, in principle, a solvable system, but it has been found heuristically that certain choices cannot be handled.

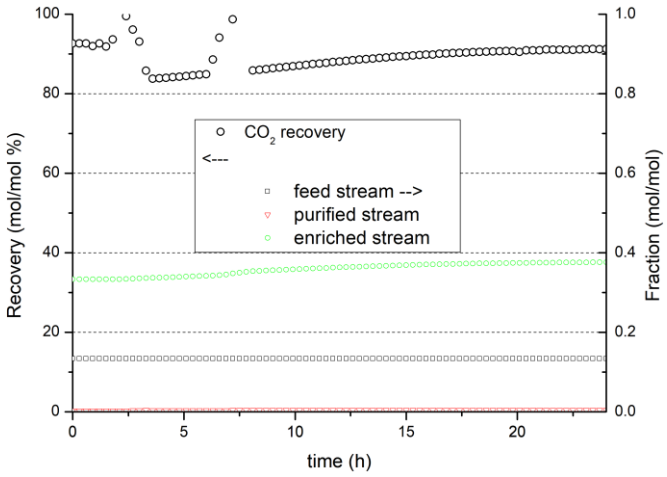

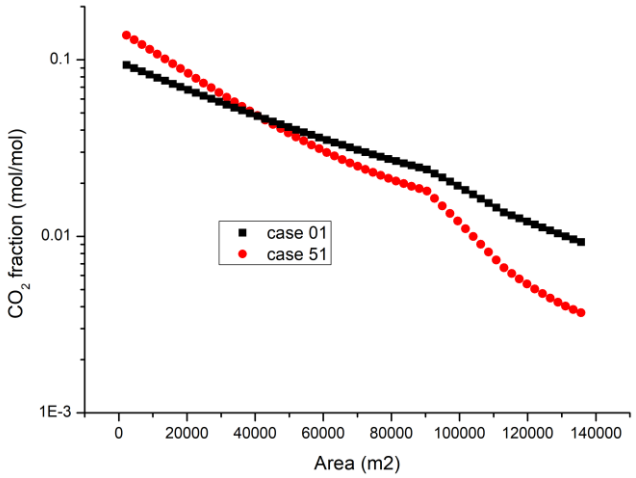

Figure 8: CO_2 recovery and mole fraction for dynamic 5. Comparison between the retentate-side CO_2 fractions with (case 01) and without (case 51) air recycle.

Figure 8 represents the CO_2 recovery for the fifth and sixth dynamic run, together with the concentration level achievable in the carbon-enriched stream. Though the final CO_2 concentration for these simulations is relatively low, the results are aligned with what reported in the literature at similar permeate vacuum levels [30], also considering that the flue gas purification predicted by the present calculus is, on the other hand, very good (CO_2 < 2% wt). Also the qualitative correlation between permeate pressure and stream flow is in agreement with published pilot-plant data [39]. Working pressures of 5 – 6 bars for the feed section have been tested also by Wu et al. [40], who used membranes with a higher permeability but a similar selectivity with respect to the values obtained in this work, keeping the permeate side at atmospheric level. Their findings for a single membrane stack are in line with the recovery/purity outcomes of the 1st co-current block without sweep air-injections simulated in this work (Figure 9). Single-pass enrichments below 40% and 50%, at very high recovery values, have also been calculated by Franz et al. [41] and by Brinkman et al. [42], respectively.

On the other hand, the tested case with sweep air recirculation yields lower CO_2 concentration after each co-current stage. The greatest difference, with respect to other cited simulation works, is the CO_2 dilution foreseen by the present calculation as the waste gas purification proceeds, due to the ever-increasing transport of N_2 through the membrane. This is due essentially to two factors: the relatively high pressure ratio adopted (which determines an appreciable driving force for all species), and the arrangement between the first and second membrane sections, which is designed to achieve a low CO_2 fraction in the wastes rather than a high CO_2 purity in the permeate.

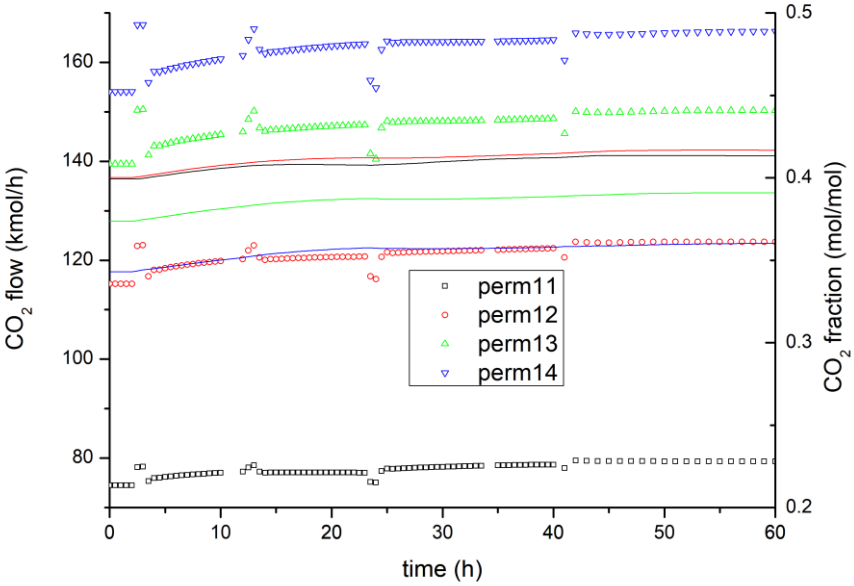

301

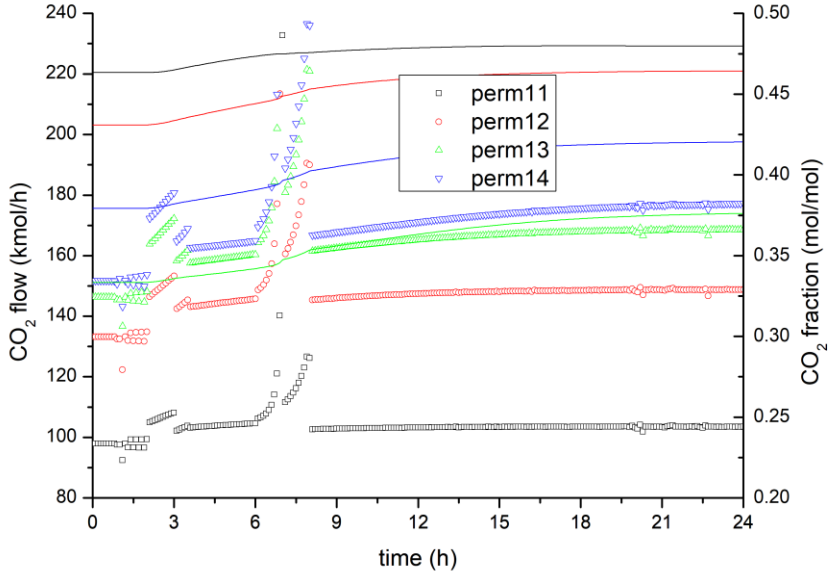

302

303 Figure 9: CO_2 flows (symbols, left axis) and fractions (lines, right axis) for the co-current cascade in dynamic

304 simulations no. 1(top) and 5 (bottom).

305

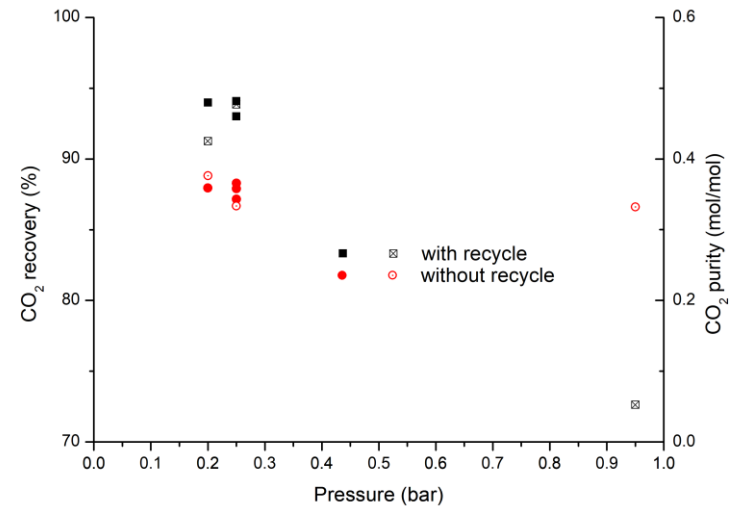

306

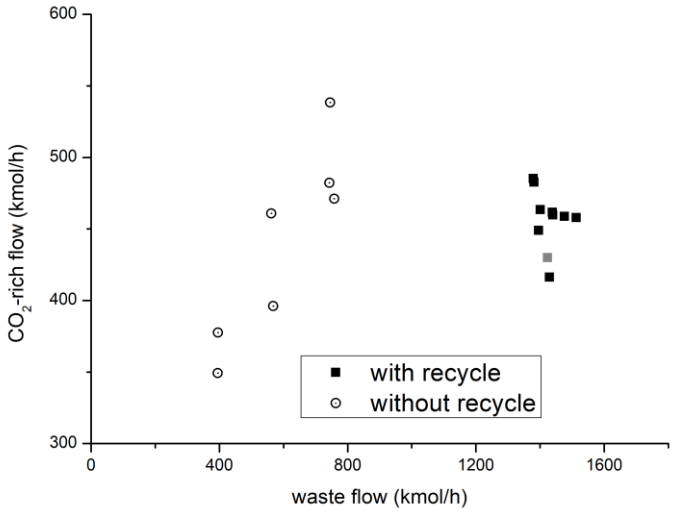

307

308 Figure 10: (top) CO_2 recovery (filled markers) and purity (empty markers) as a functions of pressure; (down) CO_2 flow

309 as function of waste flow (the grey square is a doubtful output).

310

311 Considering a selection of quasi-steady states (from Table 6), it is found that the carbon recovery is

312 sensitive to the permeate vacuum (i.e. to the pressure ratio, Figure 10), but is stabilized if the recycle

313 air is added: in this case the CO_2-rich flow becomes independent by the purified flues flow (Figure

314 10), while otherwise the two streams are proportional to one another. The achieved purity is not

315 affected appreciably by the tested process variables, because it is linked to the selectivity.

316

Conclusions

A dynamic model to describe the operation of a hollow-fiber membrane has been validated for the case of N_2-O_2 separation, and extended to the N_2-CO_2-H_2O mixture. In order to simulate dynamically the whole process of combustion gases purification, equations for compressors and condensers have been added, and all the blocks linked into process flowsheets, obtaining a scaled-up simulation for the whole fuel purification. The treated gas quantity and the total membranes that are needed have been increased adopting the largest compressor characteristic curve available in detail as constraint: this grants the best compromise between the needed units (14 compressors) and the model reliability. The dynamic calculation helps to foresee undesired oscillations in the main process outcome (CO_2 residue in the purified stream), and the delays caused by the blocks volume. The steady state results are comparable with other simulation and plant data available: the proposed design, anyway, is not aimed to CO_2 purification, so the membrane layout has been optimized to grant <1% mol in the exit flues, despite the low concentration < 40% mol in the carbon-rich stream.

A layout featuring air recycle can stabilize the system dynamics, keeping the CO_2 content variation within 30% and its oscillation within 150% (dynamic 4), a once-through layout yields variations as high as 200-300%, but it needs roughly half the membrane area to achieve the same purification targets. This poses the basis to evaluate the compromise between additional installation costs and possible transient off-target performance of the plant.

Acronyms and Symbols

f	Friction factor	A	Hydraulic Area
k	Vapor velocity correction	Cv	Valve coefficient
i	Species index	D	Hydraulic diameter
n	Moles	F	Feed mass flow
p	Partial pressure	J	Molar flux

u	Velocity	L	Liquid mass flow
v	Volume	P	Total pressure
x	Liquid mole fraction	Q	Thermal power
y	Gas mole fraction	R	Gas constant
z	Molar fraction	S	Permeation surface
ε	Rugosity	T	Temperature
φ	Flow factor	U	Heat exchange coefficient
γ	Heat capacities ratio	V	Vapor mass flow
η	Efficiency	W	Work
ρ	Mass density	GPU	Gas-Permeation Unit
		Re	Reynold number
		RET	Retentate
		PER	Permeate
		PM	Molar weight

Acknowledgments

A. Tripodi gratefully acknowledges MUR for funding its RTDA position in the frame of the project Programma Operativo Nazionale "Ricerca e Innovazione" 2014/2020 to deliver research on "Green" topics.

I. Rossetti gratefully acknowledges the financial contribution of Fondazione Cariplo through the grant 2021-0855 – "SCORE - Solar Energy for Circular CO_2 Photoconversion and Chemicals Regeneration", funded in the frame of the Circular Economy call 2021.

I. Rossetti acknowledges Università degli Studi di Milano for support through the grant PSR 2021 - GSA - Linea 6 "One Health Action Hub: University Task Force for the resilience of territorial ecosystems".

This study was carried out within the Agritech National Research Center and received funding from the European Union Next-GenerationEU (PIANO NAZIONALE DI RIPRESA E RESILIENZA

(PNRR) – MISSIONE 4 COMPONENTE 2, INVESTIMENTO 1.4 – D.D. 1032 17/06/2022, CN00000022). This manuscript reflects only the authors' views and opinions, neither the European Union nor the European Commission can be considered responsible for them. I. Rossetti and M. Tommasi acknowledge specifically the participation and funding of Tasks 8.2.3, 8.3.2 and 8.4.1.

Dedication

This paper is dedicated to the memory of Prof. Lucio Forni, formerly professor at Università degli Studi di Milano, passed away at the end of December 2022. I. Rossetti, as former student and colleague, gratefully remembers all the teachings and the moments spent together.

References

[1] Araújo O de QF, de Medeiros JL. Carbon capture and storage technologies: present scenario and drivers of innovation. Curr Opin Chem Eng 2017;17:22–34. https://doi.org/10.1016/j.coche.2017.05.004.

[2] Ochedi FO, Liu Y, Adewuyi YG. State-of-the-art review on capture of CO2 using adsorbents prepared from waste materials. Process Saf Environ Prot 2020;139:1–25. https://doi.org/10.1016/j.psep.2020.03.036.

[3] Medhat A. Nemitallah, Mohamed A. Habib, Hassan M. Badr, Syed A. Said, Aqil Jamal, Rached Ben-Mansour, Esmail M. A. Mokheimer KM. Oxy-fuel combustion technology: current status, applications, and trends. Int J Energy Res 2017;41:1670–708. https://doi.org/10.1002/er.3722.

[4] Merkel TC, Lin H, Wei X, Baker R. Power plant post-combustion carbon dioxide capture: An opportunity for membranes. J Memb Sci 2010;359:126–39. https://doi.org/10.1016/j.memsci.2009.10.041.

[5] Castel C, Bounaceur R, Favre E. Membrane Processes for Direct Carbon Dioxide Capture

From Air: Possibilities and Limitations. Front Chem Eng 2021;3:1–15. https://doi.org/10.3389/fceng.2021.668867.

[6] Font-Palma C, Cann D, Udemu C. Review of Cryogenic Carbon Capture Innovations and Their Potential Applications. C 2021;7:58. https://doi.org/10.3390/c7030058.

[7] Kotowicz J, Chmielniak T, Janusz-Szymańska K. The influence of membrane CO2 separation on the efficiency of a coal-fired power plant. Energy 2010;35:841–50. https://doi.org/10.1016/j.energy.2009.08.008.

[8] Luis P, Van der Bruggen B. The role of membranes in post-combustion CO2 capture. Greenh Gases Sci Technol 2013;3:318–37. https://doi.org/10.1002/ghg.1365.

[9] Wang R, Zhang HY, Feron PHM, Liang DT. Influence of membrane wetting on CO2 capture in microporous hollow fiber membrane contactors. Sep Purif Technol 2005;46:33–40. https://doi.org/10.1016/j.seppur.2005.04.007.

[10] Politecnico di Milano - Alstom UK. CArbon-free Electricity by SEWGS: Advanced materials, Reactor-, and process design - D4.9 European best practice guidelines for assessment of CO2 capture technologies. 2011.

[11] Bhown AS, Freeman BC. Analysis and status of post-combustion carbon dioxide capture technologies. Environ Sci Technol 2011;45:8624–32. https://doi.org/10.1021/es104291d.

[12] Kárászová M, Zach B, Petrusová Z, Červenka V, Bobák M, Šyc M, et al. Post-combustion carbon capture by membrane separation, Review. Sep Purif Technol 2020;238. https://doi.org/10.1016/j.seppur.2019.116448.

[13] Li L, Ma G, Pan Z, Zhang N, Zhang Z. Research progress in gas separation using hollow fiber membrane contactors. Membranes (Basel) 2020;10:1–20. https://doi.org/10.3390/membranes10120380.

[14] Wan CF, Yang T, Lipscomb GG, Stookey DJ, Chung TS. Design and fabrication of hollow fiber membrane modules. J Memb Sci 2017;538:96–107. https://doi.org/10.1016/j.memsci.2017.05.047.

401 [15] Yan Y, Zhang Z, Zhang L, Chen Y, Tang Q. Dynamic modeling of biogas upgrading in hollow
402 fiber membrane contactors. Energy and Fuels 2014;28:5745–55.
403 https://doi.org/10.1021/ef501435q.
404 [16] Cui Z, Demontigny D. Part 7: A review of CO2 capture using hollow fiber membrane
405 contactors. Carbon Manag 2013;4:69–89. https://doi.org/10.4155/cmt.12.73.
406 [17] He X, Fu C, Hägg MB. Membrane system design and process feasibility analysis for
407 CO2capture from flue gas with a fixed-site-carrier membrane. Chem Eng J 2015;268:1–9.
408 https://doi.org/10.1016/j.cej.2014.12.105.
409 [18] Alshehri A, Khalilpour R, Abbas A, Lai Z. Membrane systems engineering for post-
410 combustion carbon capture. Energy Procedia 2013;37:976–85.
411 https://doi.org/10.1016/j.egypro.2013.05.193.
412 [19] Walawender WP, Stern SA. Analysis Of Membrane Separation Parameters. Ii. Countercurrent
413 And Cocurrent Flow In A Single Permeation Stage. Sep Sci 1972;7:553–84.
414 https://doi.org/10.1080/00372367208056054.
415 [20] Chabanon E, Roizard D, Favre E. Modeling strategies of membrane contactors for post-
416 combustion carbon capture: A critical comparative study. Chem Eng Sci 2013;87:393–407.
417 https://doi.org/10.1016/j.ces.2012.09.011.
418 [21] Belaissaoui B, Willson D, Favre E. Membrane gas separations and post-combustion carbon
419 dioxide capture: Parametric sensitivity and process integration strategies. Chem Eng J
420 2012;211–212:122–32. https://doi.org/10.1016/j.cej.2012.09.012.
421 [22] Kusuma VA, Venna SR, Wickramanayake S, Dahe GJ, Myers CR, O'Connor J, et al. An
422 automated lab-scale flue gas permeation membrane testing system at the National Carbon
423 Capture Center. J Memb Sci 2017;533:28–37. https://doi.org/10.1016/j.memsci.2017.02.051.
424 [23] Coker DT, Freeman BD, Fleming GK. Modeling multicomponent gas separation using hollow-
425 fiber membrane contactors. AIChE J 1998;44:1289–302.
426 https://doi.org/10.1002/aic.690440607.

[24] Neurath Power Station. RWE Glob n.d.

[25] Pohlmann J, Bram M, Wilkner K, Brinkmann T. Pilot scale separation of CO2 from power plant flue gases by membrane technology. Int J Greenh Gas Control 2016;53:56–64. https://doi.org/10.1016/j.ijggc.2016.07.033.

[26] Finlayson BA. Introduction to Chemical Engineering Computing. John Wiley & Sons; 2012.

[27] Venturini M. Development and experimental validation of a compressor dynamic model. J Turbomach 2005;127:599–608. https://doi.org/10.1115/1.1928935.

[28] Ren LX, Chang FL, Kang DY, Chen CL. Hybrid membrane process for post-combustion CO2 capture from coal-fired power plant. J Memb Sci 2020;603:118001. https://doi.org/10.1016/j.memsci.2020.118001.

[29] Scholz M, Harlacher T, Melin T, Wessling M. Modeling gas permeation by linking nonideal effects. Ind Eng Chem Res 2013;52:1079–88. https://doi.org/10.1021/ie202689m.

[30] White LS, Wei X, Pande S, Wu T, Merkel TC. Extended flue gas trials with a membrane-based pilot plant at a one-ton-per-day carbon capture rate. J Memb Sci 2015;496:48–57. https://doi.org/10.1016/j.memsci.2015.08.003.

[31] Hasse D, Kulkarni S, Sanders E, Corson E, Tranier JP. CO2 capture by sub-ambient membrane operation. Energy Procedia 2013;37:993–1003. https://doi.org/10.1016/j.egypro.2013.05.195.

[32] Green DW, Perry RH. Perry's Chemical Engineers' Handbook. 8th ed. The McGraw-Hill Companies, Inc; 2008.

[33] Mishina H, Gyobu I. Performance Investigations of Large Capacity Centrifugal Compressors. Am Soc Mech Eng 1978:1–11.

[34] Han Y, Ho WSW. Polymeric membranes for CO2 separation and capture. J Memb Sci 2021;628. https://doi.org/10.1016/j.memsci.2021.119244.

[35] Merkel T. Membrane Process to Sequester CO2 from Power Plant Flue Gas. FINAL REPORT. Award Number DE-NT0005312 2011;3:3–4.

[36] Scholz M, Alders M, Lölsberg J, Wessling M. Dynamic process simulation and process control

of biogas permeation processes. J Memb Sci 2015;484:107–18. https://doi.org/10.1016/j.memsci.2015.03.008.

[37] Bringhenti C, Tomita JT, Barbosa JR. Performance study of a 1 MW gas turbine using variable geometry compressor and turbine blade cooling. Proc ASME Turbo Expo 2010;3:703–10. https://doi.org/10.1115/GT2010-22867.

[38] Merkel TC, Wei X, He Z, White LS, Wijmans JG, Baker RW. Selective exhaust gas recycle with membranes for CO2 capture from natural gas combined cycle power plants. Ind Eng Chem Res 2013;52:1150–9. https://doi.org/10.1021/ie302110z.

[39] White LS, Amo KD, Wu T, Merkel TC. Extended field trials of Polaris sweep modules for carbon capture. J Memb Sci 2017;542:217–25. https://doi.org/10.1016/j.memsci.2017.08.017.

[40] Wu H, Li Q, Sheng M, Wang Z, Zhao S, Wang J, et al. Membrane technology for CO2 capture: From pilot-scale investigation of two-stage plant to actual system design. J Memb Sci 2021;624:119137. https://doi.org/10.1016/j.memsci.2021.119137.

[41] Franz J, Schiebahn S, Zhao L, Riensche E, Scherer V, Stolten D. Investigating the influence of sweep gas on CO2/N2 membranes for post-combustion capture. Int J Greenh Gas Control 2013;13:180–90. https://doi.org/10.1016/j.ijggc.2012.12.008.

[42] Brinkmann T, Pohlmann J, Bram M, Zhao L, Tota A, Jordan Escalona N, et al. Investigating the influence of the pressure distribution in a membrane module on the cascaded membrane system for post-combustion capture. Int J Greenh Gas Control 2015;39:194–204. https://doi.org/10.1016/j.ijggc.2015.03.010.